Earth and Planetary Science Letters 574 (2021) 117163

Contents lists available at ScienceDirect

Earth and Planetary Science Letters

www.elsevier.com/locate/epsl

Release from biogenic particles, benthic fluxes, and deep water circulation control Cr and δ^{53}Cr distributions in the ocean interior

David J. Janssen [a,*], Jörg Rickli [a,b], April N. Abbott [c,1], Michael J. Ellwood [d], Benjamin S. Twining [e], Daniel C. Ohnemus [f], Philipp Nasemann [a], Delphine Gilliard [a,g], Samuel L. Jaccard [a,g]

[a] University of Bern, Institute of Geological Sciences & Oeschger Center for Climate Change Research, Baltzerstrasse 1-3, 3012 Bern, Switzerland
[b] Institute of Geochemistry and Petrology, ETH Zürich, Zürich, Switzerland
[c] Department of Earth & Environmental Sciences, Macquarie University, Sydney, NSW, Australia
[d] Research School of Earth Sciences, Australian National University, Canberra, Australia
[e] Bigelow Laboratory for Ocean Sciences, East Boothbay, ME, USA
[f] University of Georgia, Skidaway Inst. of Oceanography, Dept. of Marine Sciences, Savannah, GA, USA
[g] University of Lausanne, Institute of Earth Sciences, Lausanne, Switzerland

ARTICLE INFO

Article history:
Received 12 March 2021
Received in revised form 2 August 2021
Accepted 13 August 2021
Available online 10 September 2021
Editor: L. Derry

Keywords:
chromium
chromium isotopes
GEOTRACES
paleoproxy
biogeochemical cycling
benthic flux

ABSTRACT

Chromium (Cr) has shown promise as a paleoceanographic proxy due to the redox-driven control of dissolved Cr concentrations ([Cr]) and stable isotope composition (δ^{53}Cr). To improve the mechanistic understanding of Cr cycling in the modern ocean and strengthen its potential proxy applications, we present new data from regeneration incubations, bottom and sediment pore waters, and a compilation of intermediate and deep water data. While Cr removal and biological export from the surface ocean is associated with organic carbon export, the deep water release of dissolved Cr from sinking particles is not directly dependent on organic carbon respiration, as indicated by differing trends between Cr, oxygen utilization and the regeneration of organic-associated macronutrients (e.g. N, P). Pore water and bottom water data demonstrate that benthic Cr fluxes are locally important and may be significant globally. The pore water dissolved Cr flux at our $CaCO_3$-rich site is likely driven by the re-release of Cr scavenged from the water column by sinking particles, with minor contributions from lithogenic phases. We argue this is consistent with the highest open ocean [Cr] to date being found in the water column below oxygen minimum zones, likely reflecting the release of scavenged Cr in deep waters or surface sediments. Chromium released from suspended particles and surface sediments follows the global δ^{53}Cr–[Cr] array, supporting the proposed role of biological export and regeneration in shaping global Cr and δ^{53}Cr distributions. Global intermediate and deep water [Cr], δ^{53}Cr and Cr:macronutrient relationships are thus shaped by a synergy of circulation patterns, water mass mixing, a deep Cr regeneration cycle, and benthic Cr sources. A biogenic control on global Cr distributions indicates that sedimentary Cr records may reflect biogenic as well as O_2-dependent processes, while more research is needed to assess sediment Cr record fidelity based on an active diagenetic cycle.

1. Introduction

Oceanic distributions of dissolved Cr show nutrient-type behavior, generally resembling primary macro- and micronutrients, though with muted surface depletions and enrichments at depth (e.g. Campbell and Yeats, 1981; Jeandel and Minster, 1987). Thermodynamic calculations predict that oxidized Cr(VI), a soluble oxyanion with low particle reactivity (Semeniuk et al., 2016), should account for all dissolved Cr in the oxygenated ocean (Elder-

* Corresponding author.
E-mail addresses: david.janssen@geo.unibe.ch (D.J. Janssen), joerg.rickli@erdw.ethz.ch (J. Rickli), abbot152@d.umn.edu (A.N. Abbott), michael.ellwood@anu.edu.au (M.J. Ellwood), btwining@bigelow.org (B.S. Twining), dan@uga.edu (D.C. Ohnemus), philipp.nasemann@geo.unibe.ch (P. Nasemann), delphine.gilliard@students.unibe.ch (D. Gilliard), samuel.jaccard@unil.ch (S.L. Jaccard).
[1] Now at Department of Marine Sciences, Coastal Carolina University, Conway, SC, USA.

https://doi.org/10.1016/j.epsl.2021.117163

field, 1970). However, the reduced form, Cr(III), is regularly found at low levels in oxygenated seawater (e.g. Cranston, 1983; Jeandel and Minster, 1987; Achterberg and van den Berg, 1997; Janssen et al., 2020), and may constitute a major fraction of dissolved Cr in oxygen minimum zones (OMZs; e.g. Murray et al., 1983; Rue et al., 1997). Chromium(III) is relatively insoluble and readily adsorbs to mineral and organic surfaces (Cranston and Murray, 1978; Mayer et al., 1984). Therefore redox transformations play a central role in Cr biogeochemical cycling. Iron(II) is an important Cr(VI) reductant in natural aquatic systems (Pettine et al., 1998), and Mn oxides (MnOx) are a primary Cr(III) oxidant (van der Weijden and Reith, 1982; Miletto et al., 2021), especially in Mn-rich environments such as sediments (Oze et al., 2007).

The main dissolved Cr removal processes in the ocean, both involving Cr reduction followed by particle scavenging, are in OMZs and through biologically-mediated export (e.g. Murray et al., 1983; Scheiderich et al., 2015). Chromium removal in OMZs has been reported in the eastern tropical North Pacific (ETNP) (Murray et al., 1983; Rue et al., 1997; Moos et al., 2020) and the eastern tropical South Pacific (ETSP) (Nasemann et al., 2020). Correlations between Cr and particulate organic carbon in sinking particles (Connelly et al., 2006), Cr(III) adsorption onto phytoplankton (Semeniuk et al., 2016), and agreements between dissolved Cr deficits and productivity-based inferred removal (Janssen et al., 2020) support a Cr sink associated with biological export. However, the subtle gradients in [Cr] depth profiles suggest that release from biogenic particles is relatively minor (e.g. Scheiderich et al., 2015; Goring-Harford et al., 2018; Moos and Boyle, 2019; Rickli et al., 2019), and circulation plays an important role in shaping distributions (e.g. Scheiderich et al., 2015; Goring-Harford et al., 2018; Rickli et al., 2019). Elevated bottom water [Cr] suggests surface to deep [Cr] gradients may be influenced by a flux from marine sediments (Murray et al., 1983; Jeandel and Minster, 1987), consistent with shallow pore water [Cr] enrichments on the California shelf, assumed to reflect release from organic matter (Shaw et al., 1990).

Chromium redox transformations are accompanied by isotopic fractionation. While fractionation patterns during Cr oxidation are variable (Zink et al., 2010; Miletto et al., 2021), reduction consistently enriches light isotopes in Cr(III) (e.g. Wanner and Sonnenthal, 2013). The redox control on [Cr] and δ^{53}Cr makes δ^{53}Cr a potentially powerful tracer of paleoredox conditions, especially in early earth studies (e.g. Frei et al., 2009). However, application and interpretation of δ^{53}Cr records require an accurate mechanistic understanding of the process(es) that control Cr budgets and isotopic fractionation in terrestrial environments, the ocean, and during incorporation into the sediment record. The systematic relationship between seawater [Cr] and δ^{53}Cr suggests that redox transformations likely control oceanic distributions of δ^{53}Cr (Scheiderich et al., 2015; Goring-Harford et al., 2018; Moos and Boyle, 2019; Moos et al., 2020; Rickli et al., 2019; Janssen et al., 2020; Nasemann et al., 2020) implying an effective isotope enrichment factor (ε) of approximately $-0.7‰$ associated with Cr reduction and removal. Recent δ^{53}Cr and [Cr] data demonstrate fractionation associated with biologically driven Cr removal in the open ocean (Janssen et al., 2020). Similarly, Cr removal in shelf settings (Goring-Harford et al., 2018), as well as in OMZs (Moos et al., 2020; Nasemann et al., 2020; Huang et al., 2021) can result in isotopic fractionation. However, isotope fractionation factors for these removal processes remain poorly constrained.

To address uncertainties in the modern ocean Cr budget and the role of biogenic processes in seawater δ^{53}Cr distributions, we present dissolved [Cr], δ^{53}Cr and [Cr(III)] from shipboard incubations, new intermediate and deep water [Cr] and δ^{53}Cr from eight research expeditions in the Southern, Pacific and Atlantic Oceans, and pore water [Cr] data from the Tasman Sea.

2. Oceanographic background - Southern Ocean intermediate and deep waters and their advection into the Pacific and Atlantic Oceans

The Southern Ocean is the formation site for much of the global deep and intermediate waters, including Antarctic Intermediate Water (AAIW) and Upper and Lower Circumpolar Deep Water (U/L-CDW). The extent to which these waters penetrate into lower latitudes in the Pacific and Atlantic Oceans varies depending on formation sites, bathymetry, and the prevalence of other water masses.

AAIW is reflected in salinity minima in depth profiles, although this erodes with northward transport, and it is found at neutral densities $\sim 27 < \gamma^{\eta} < \sim 27.4$ (Orsi et al., 1995; Talley et al., 2011; Bostock et al., 2013). AAIW flows northward to the tropical South Pacific ($\sim$10-15°S) where it mixes with Equatorial Pacific Intermediate Water (Bostock et al., 2013). Atlantic AAIW is diluted by mixing during northward transport, as evidenced by increased salinity, and reaches a maximum extent slightly beyond the equator (Suga and Taley, 1995). Tropical Atlantic AAIW is found at a depth of around 700-800 m discernible by low salinity ($\sim$34.20-34.40) and high O_2 ($\geq$190 µmol kg^{-1}) south of 20°S.

The deep waters of the Pacific Ocean comprise UCDW, LCDW and PDW, the latter of which is largely found at similar densities as UCDW ($\gamma^{\eta} < 28.0$; T > 1.5 °C; S < 34.65 PSU) and is formed as the colder, more saline and more oxygen rich LCDW ($\gamma^{\eta} > 28.0$) is upwelled and mixed throughout Pacific (Orsi et al., 1995; Kawabe and Fujio, 2010; Talley et al., 2011). Densities occupied by UCDW transition to predominantly PDW in the tropical South to subtropical North Pacific. LCDW extends into the North Pacific along the western side of the basin, and the northernmost reaches are characterized by elevated [$Si(OH)_4$] ($\geq$170 µmol kg^{-1}) (Kawabe and Fujio, 2010). CDW enters the South Atlantic below AAIW and can be dominant as far north as $\sim$25°S, but its relative contribution weakens as the water mass continues northward, with CDW accounting for $\leq$50% of deep waters in the tropical Atlantic (Larqué et al., 1997).

3. Methods

Intermediate and deep water [Cr] and δ^{53}Cr samples were collected on RV *Investigator* expeditions IN2018_V02 (Mar-2018) and IN2018_V04 (Sept-Oct 2018), ACE Legs 1 (Dec-2016 to Jan-2017) and 2 (Jan-2017 to Feb-2017), GEOTRACES section GP13 (Australian leg, May-June 2011), RV *Meteor* cruise M77/4 (Jan-Feb 2009), Line P cruise 2012-13 (Aug-2012), and RV *Discovery* cruise DY110 (Oct-Nov 2019) (Fig. 1). Further analyses were performed on bottom and pore waters (IN2018V_04) and on samples from shipboard regeneration incubation experiments (IN2018V_02).

3.1. Incubation design and sampling

Incubation regeneration experiments were carried out at the Southern Ocean Time Series (SOTS) site, in the open subantarctic Southern Ocean south of Tasmania (IN2018_V02, $\sim$4600 m water depth) in acid-cleaned 20 L LDPE cubitainers with Teflon-lined caps. Three experiments were conducted, with differences in incubation temperature and the particle collection depth (supplemental material). All experiments used particles from below the chlorphyll max ($\sim$60 m depth) and at or below the mixed layer depth ($\sim$90 m depth). Each experiment consisted of two treatments, each in triplicate. Cubitainers were filled with filtered (0.2 µm) surface ($\sim$5 m) seawater collected using a trace metal-clean tow fish, and aliquots were collected for initial (T_0) nutrients, [Cr] and δ^{53}Cr before particle inoculation. Filled cubitainers were stored in the dark at 1 °C until inoculating with particles (within 8 hours of filling).

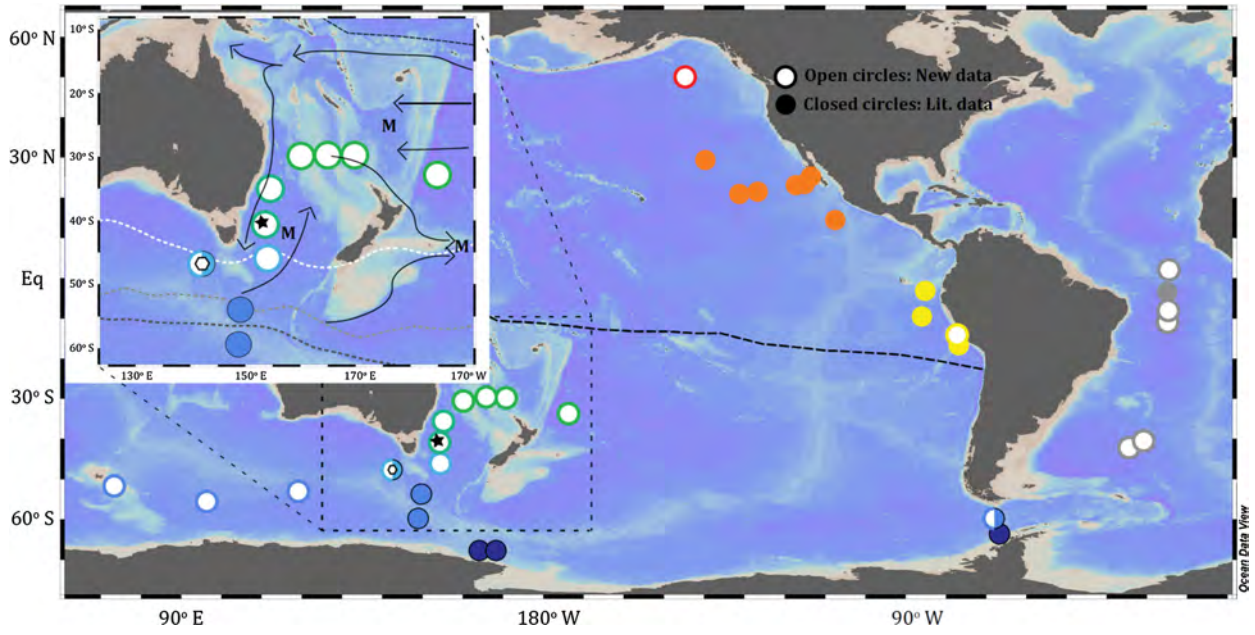

Fig. 1. Map of sampling locations. Station locations are shown for new data (open circles) and literature data (filled circles). Split circles indicate locations with both new and literature data. Full data tables can be found in the supplemental material. The black star denotes the location of the multicore site, where bottom and pore waters were collected. The northernmost extent of AAIW as a primary water mass component in the Pacific Ocean (Bostock et al., 2013), is shown as a dashed black line. The inset shows the subantarctic Southern Ocean, the Tasman Sea (located between Australia and New Zealand) and the subtropical southwestern Pacific, the sites for most of the new data. The flow paths of AAIW are shown in the inset as black arrows, and M denotes regions of enhanced AAIW mixing (Bostock et al., 2013). Dashed white and grey lines indicate representative fronts of the Southern Ocean (white – the Subtropical Front, light grey – the Subantarctic Front, dark grey – the Polar Front; Orsi et al., 1995). (For interpretation of the colors in the figure(s), the reader is referred to the web version of this article.)

Ambient suspended particle samples from the oxic water column were collected onto acid-cleaned 1 µm polycarbonate filters using in-situ pumps (McLane). Particles were resuspended from these filters, forming a particle-rich slurry that was added to the individual cubitainers to result in particulate concentrations approximately 2-4 fold above natural levels. Because only resuspended particles were added to the incubations, the high Cr blanks associated with many filter materials (e.g. Scheiderich et al., 2015) will not impact the incubations.

Particle-inoculated cubitainers were incubated in the dark at either 4 °C (ambient) or 1 °C (cold treatment) for five days, with three subsampling time points. For subsampling, the cubitainers were transported to a Class 100 clean van, gently mixed, and subsampled into acid-cleaned LDPE bottles (for trace metals) or polycarbonate tubes (for macronutrients). Subsamples for trace metals were transported to a laminar flow hood and filtered through acid-cleaned 0.4 µm polycarbonate filters using a Teflon vacuum filtration apparatus (Savillex). Loss of Cr to container walls has been shown to be minimal over short timeframes (e.g. Semeniuk et al., 2016) and was not considered here. Chemically-labile particulate metal and P concentrations were determined with magnetic-sector ICP-MS following solubilisation with a heated mixture of reductant (hydroxylamine hydrochloride) and weak acid (acetic acid) designed to dissolve biogenic material and Mn and Fe oxides (Berger et al., 2008). Analytical procedures followed those previously described in Rauschenberg and Twining (2015).

3.2. Bottom water, pore water and sediment sampling

Pore water and bottom water samples for this study were collected from a multicore deployment near Station PS3 in the Tasman Sea (Fig. 1, 3349 m water depth). Cores for pore water, bottom water, and sediment samples were processed in an N_2 environment. A bottom water sample was extracted from the core tube approximately 10 cm above the sediment-water interface using an acid-cleaned rubber-free syringe and filtering through a 0.45 µm syringe filter into an acid-cleaned LDPE bottle. The bottom water was visibly clear and free from sediment resuspension, and the sediment surface appeared undisturbed.

Pore water samples were collected following procedures outlined in Abbott et al. (2015). In brief, 1 cm depth intervals were placed into acid-cleaned centrifuge tubes in a glove bag, sealed, then centrifuged at 4500 rpm for 20 minutes. The pore water (supernatant) was extracted from centrifuged samples and filtered as outlined for bottom water. The samples were acidified, stored and analyzed for [Cr] by isotope dilution as described in section 3.6. Pore water subsamples were diluted 40x and [Fe] and [Mn] were determined by high resolution inductively coupled plasma–mass spectrometry (HR-ICP-MS) (Element XR, ThermoScientific) at the Australian National University. Centrifuged sediments were stored frozen until freeze-dried, then analyzed for bulk composition ($CaCO_3$, organic matter, lithogenic material; supplemental material).

3.3. New and literature data from the Southern, Pacific and Atlantic Oceans

We present a compilation of new and literature [Cr] data in Southern-sourced intermediate and deep waters across the Southern, Pacific, and Atlantic Oceans (Fig. 1). Literature [Cr] data were not included if: (1) hydrographical data (temperature, salinity) are missing, (2) the data have not been peer-reviewed, or (3) later publications identified them as suspect or incorrect.

We add 12 samples from the Indian Sector of the Southern Ocean (ACE Leg 1) and one sample from the Drake Passage (ACE Leg 2) to [Cr] and δ^{53}Cr available from the Pacific Sector of the Southern Ocean (Rickli et al., 2019) to further constrain the composition of southern-sourced end-members. The Drake Passage sample constrains the characteristics of intermediate waters entering the Atlantic Ocean.

We present data from five stations in the subantarctic Southern Ocean and the Tasman Sea (IN2018V_02 and IN2018V_04, 26 sam-

ples) and four stations in the Tasman Sea and subtropical South Pacific (GEOTRACES section GP13, 12 samples) in order to characterize waters advecting northward into the Pacific Ocean.

Four new samples from below one of the most intense OMZs in the global ocean (ETSP near Peru; M77/4) are added to existing ETSP (Nasemann et al., 2020), ETNP OMZ (Murray et al., 1983; Rue et al., 1997), and subtropical North Pacific (Moos and Boyle, 2019) data. Additionally, we present four new samples from a profile in the subarctic North Pacific (Line P 2012-13) to characterize the northern extent of deep water in the Pacific Ocean. Previous subarctic North Pacific [Cr] literature data in PDW and LCDW (Cranston, 1983; Mugo and Orians, 1993) show a clear offset from recent high-precision data and are not used (see Table S11).

To follow the northward advection of AAIW into the equatorial Atlantic, we present seven samples from five stations along a meridional transect (DY110). Additional literature data from the Atlantic are limited, with only one sample within AAIW (station 11.5, Goring-Harford et al., 2018) and no available CDW data.

3.4. Water column dissolved Cr sampling

IN2018_V02, IN2018_V04, and GP13 samples were collected using an autonomous trace metal clean rosette system and gravity filtered through acid-cleaned 0.2 µm filters (Pall Acropak) into acid cleaned LDPE bottles in a class 100 clean van. IN2018 samples were acidified to pH < 2 (2 mL L^{-1} sub-boiling distilled concentrated HCl) on land and stored for 3-26 months before analysis. GP13 samples were stored frozen until 2019, at which point they were thawed, acidified as for IN2018 samples, and stored at least 7 months before analysis. DY110 samples were collected with a conventional CTD-rosette, gravity filtered through acid-cleaned 0.2 µm filters (Pall Acropak) acidified to pH ≈ 2 (1 mL L^{-1} concentrated HCl), and stored for at least 3 months before analysis. Sampling and sample handling are discussed in detail elsewhere for ACE (Rickli et al., 2019), M77/4 (Nasemann et al., 2020) and Line P (Janssen and Cullen, 2015).

3.5. Cr(III) samples

Dissolved chromium redox speciation (Cr(III)) samples were processed at sea using magnesium hydroxide ($Mg(OH)_2$) co-precipitation, then analysed by isotope dilution ICP-MS at the University of Bern following the procedures of Janssen et al. (2020) (external [Cr(III)] $1\sigma = 10\%$ RSD, Janssen et al., 2020).

3.6. Chromium concentrations and $\delta^{53}Cr$

Procedures for the determination of total dissolved Cr concentrations ([Cr]) and stable isotope composition ($\delta^{53}Cr$) are described in detail in Rickli et al. (2019), with minor modifications (see supplemental material; Janssen et al., 2020; Nasemann et al., 2020). Briefly, preliminary [Cr] for spiking purposes was determined on small sample aliquots by isotope dilution with $Mg(OH)_2$ co-precipitation followed by cation exchange chromatography. The final reported [Cr] is from $\delta^{53}Cr$ determinations, except when $\delta^{53}Cr$ samples were not available (pore waters and incubation intermediate time points). Pore water samples (0.2 mL) were dried rather than co-precipitated before chromatography. For $\delta^{53}Cr$, a 0.25-1 L sample aliquot was spiked with ^{50}Cr-^{54}Cr double spike, pre-concentrated by $Mg(OH)_2$ co-precipitation, and purified by a 2 step column chromatography.

Samples were analyzed on a ThermoFisher Neptune Plus MC-ICP-MS at the University of Bern following Rickli et al. (2019). $\delta^{53}Cr$ procedural blanks were 0.3-0.6 ng Cr and insignificant relative to sample Cr. $\delta^{53}Cr$ data are reported relative to NIST SRM 979. Internal uncertainties were generally 0.02-0.03‰ (2 SEM); external reproducibility, based on replicate analyses of seawater samples, is ±0.033 (2 SD) for $\delta^{53}Cr$ and <1% (1 RSD) for [Cr] (see Janssen et al., 2020). A Merck Cr(III) standard was run to monitor mass-spectometric accuracy ($\delta^{53}Cr = -0.426 \pm 0.027$‰, n = 9; literature: $\delta^{53}Cr = -0.443 \pm 0.022$‰, Schoenberg et al., 2008). The procedural accuracy of our method has previously been validated by an inter-laboratory comparison (Rickli et al., 2019), and the precision of seawater analyses during this study was confirmed through regular analysis of separate aliquots of OSIL seawater ($\delta^{53}Cr = 0.89 \pm 0.03$, n=11; www.osil.co.uk).

4. Results and discussion

4.1. Regeneration incubation experiments

Three incubation experiments to probe for broad, differential effects on the regeneration of trace elements were conducted at the SOTS site (subantarctic Southern Ocean, Fig. 1) within 10 days of each other, with varying experimental design (particle collection depth and incubation temperatures) and natural variability in the initial particulate regime and elemental concentrations. Only one incubation (Inc. 3, particles from 150 m depth) generated significant differences in [Cr] and $\delta^{53}Cr$ by the final time point. We focus on this incubation here, with results from Inc. 1 and 2 provided in the supplemental material (Section S1, Figure S1, Tables S3-S4). Initial particulate P (pP), Mn (pMn) and Fe (pFe) concentrations from all incubations are shown in Table S1.

Time series sediment trap data from SOTS indicate that fluxes are dominated by biogenic particles (>90%, total fluxes at 1000-3800 m = 13-21 g m^{-2} yr^{-1}, Wynn-Edwards et al., 2020), with high contributions from coccolithophores (Wilks et al., 2017), while lithogenic contributions are minor (<0.7 g m^{-2} yr^{-1}, Trull et al., 2001). Supportively, flow cam data from our incubations document a predominance of small particles (mostly ~2 µm, nearly all <6 µm), with a high abundance of flagellates (including coccolithophores, data not shown). Furthermore, POC profiles (Figure S2) and sediment trap data (Wilks et al., 2017; Wynn-Edwards et al., 2020) identify general stability in bulk particulate composition with depth from 150 m, indicating that the particles used here as broadly representative of local export.

There was minimal to no net regeneration of organic-associated macronutrients as indicated by the lack of macronutrient variability (N and P) (Fig. 2, Table S2). Chromium concentrations, [Cr(III)] and $\delta^{53}Cr$ remained stable over the first three days. However, [Cr] increased by an average of 0.46 ± 0.14 and 0.56 ± 0.18 nmol kg^{-1} (1 SD of the triplicates) by the final sampling for the ambient and cold treatments, respectively (Fig. 2), demonstrating that Cr release was independent from organic carbon respiration. Small increases in [Cr(III)] were also observed by the end of the incubation, though [Cr] increases were approximately seven times larger. Particulate Cr was probably primarily Cr(III) – Cr(III) dominates biogenic particle-adsorbed Cr, with Fe oxides playing an important role for Cr(III) scavenging (e.g. Semeniuk et al., 2016). Although carbonates may also host Cr (as Cr(VI)), the Cr content of $CaCO_3$ is very low (Remmelzwaal et al., 2019), and exported $CaCO_3$ is largely preserved with depth at this site (Wynn-Edwards et al., 2020), making carbonates unlikely to drive the observed dissolved [Cr] accumulation. Therefore, due to the small changes in [Cr(III)], particulate Cr was either oxidatively released or oxidized shortly after release.

While more observational constraints would be needed for a detailed mechanistic framework of the processes regulating Cr oxidation, we explore likely oxidants based on available data and geochemical constraints from the literature. The primary oceanic Cr(III) oxidants are MnOx (e.g. van der Weijden and Reith, 1982;

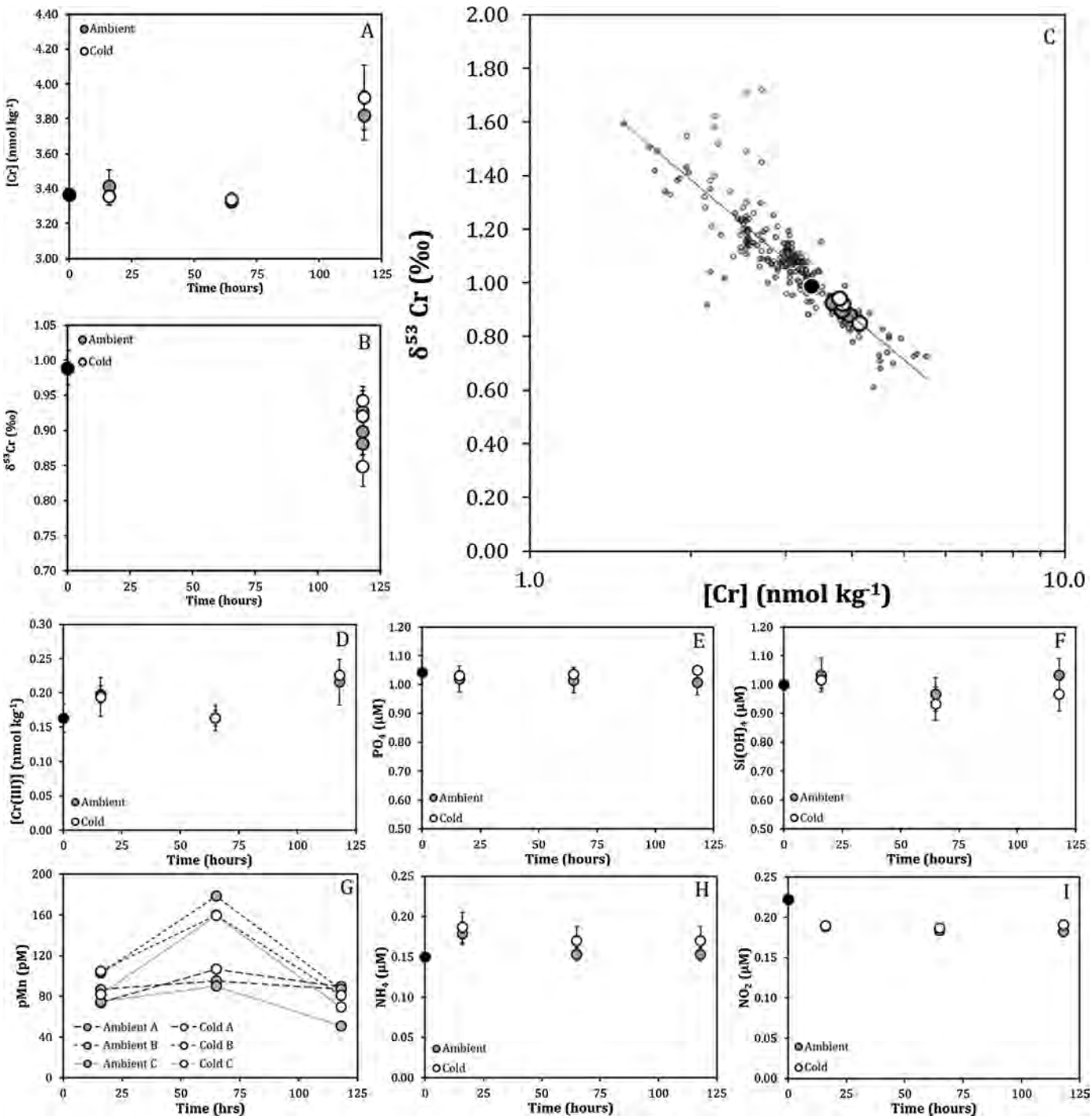

Fig. 2. Regeneration incubation data. Data for dissolved Cr concentrations (panel A), stable isotope composition (panel B) and redox speciation (panel D) are presented for regeneration incubation 3, along with macronutrients (PO_4: panel E; $Si(OH)_4$: panel F; NH_4: panel H; NO_2: panel I) and pMn (panel G). Incubation sample δ^{53}Cr and [Cr] are shown over the global array of oceanic data with a trendline fit to all the data (Panel C), demonstrating the alignment of released Cr along the global distribution. The ambient temperature (4 °C) treatment is shown as grey circles and the 1 °C treatment as white circles, with the initial dissolved water shown as a black circle.

Miletto et al., 2021) and H_2O_2 (Pettine et al., 1991). Other redox-active species (e.g. N), while present in the incubations, do not have known roles for Cr oxidation and are unlikely oxidants based on reduction potentials (Rue et al., 1997) and oceanic data showing correlations with of NO_3 reduction with Cr reduction rather than Cr oxidation (Rue et al., 1997; Moos et al., 2020; Nasemann et al., 2020).

Particles in our incubations were enriched in Mn beyond typical cellular quotas (Table S1, Twining and Baines, 2013), indicating the presence of MnOx. We also observe increasing pMn between the first and second time points, indicating further enrichment in MnOx, consistent with mid-depth scavenging of Mn (e.g. Ohnemus et al., 2019). The timing of the Cr release in Inc. 3 matches a decrease in pMn (Fig. 2), supporting Mn reduction coupled to Cr oxidation and release, though the increase in Cr(VI) stoichiometrically exceeds that suggested by pMn and the Mn(IV)-Cr(III) redox couple. Since we observe an active cycle of Mn, with first increasing and then decreasing pMn, repeated microbial Mn(II) oxidation followed by MnOx reduction with Cr(III) oxidation may explain the [Cr] accumulation above expected reaction stoichiometry. This has

Table 1
Mass balance for sedimentary Cr. Potential sources of Cr in marine sediments are compared to evaluate the origin of the benthic Cr flux. Sediment phase percentages (organic matter, $CaCO_3$, lithogenic material) are averages from the upper 4 cm (Table S6). Cr per phase is the concentration expected in each individual phase (surface phytoplankton: Martin and Knauer, 1973; $CaCO_3$: Remmelzwaal et al., 2019; upper continental crust: Rudnick and Gao, 2003). Cr contributed to bulk sediment is the Cr that each phase would contribute to the bulk sediment concentration, based on sediment phases and Cr per phase. Cr needed is the required [Cr] in the sediments (i.e. the [Cr] of particles that must be delivered to sediments) to explain the calculated diffusive Cr flux from sediments (3.2 nmol cm^{-2} yr^{-1}, Table S6), assuming a sedimentation rate in the region of 2 cm ka^{-1} (e.g. Cochran and Osmond, 1976). A sedimentation rate on the higher side of regional observations was chosen to give a minimum estimate of the Cr needed. The assumed sediment density is 1.7 g cm^{-3}.

Potential sources	Sediment phase (% of bulk)	Cr per phase (ppm)	Cr contributed to bulk sediment (ppm)	Cr needed (ppm)
Organic matter/ Surface phytoplankton	1	11.7	0.1	
$CaCO_3$	76	0.1	0.08	49
Lithogenic material/ Upper continental crust	20	90	18	

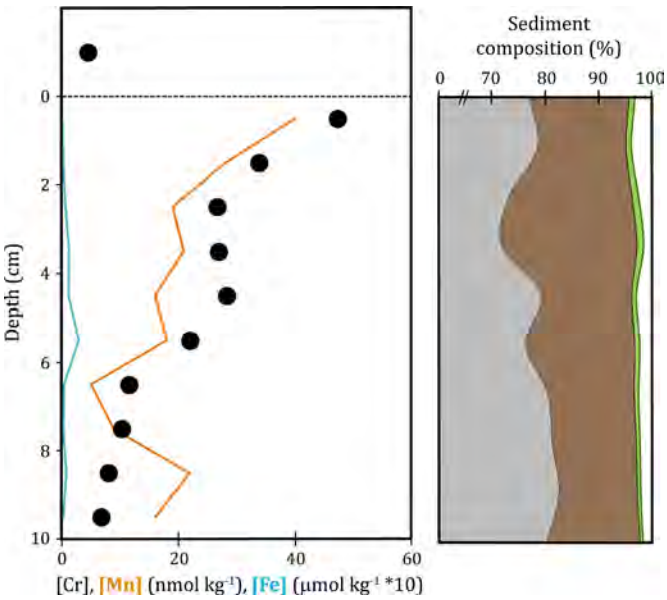

Fig. 3. Pore water [Cr] profile. The left panel shows pore water dissolved [Cr], [Mn] and [Fe] with depth in the sediment. Note that [Cr] and [Mn] are presented as nmol kg^{-1}, while Fe is presented as µmol kg^{-1} with concentrations multiplied by ten to match axis scaling (i.e. 2 µmol kg^{-1} Fe would correspond to the axis tick mark for 20 in this figure). Concentrations represent pore water concentrations in sample intervals of 1 cm. Dissolved bottom water [Cr] is shown from a sample collected approximately 10 cm above the sediment-water interface (shown as a dashed line). Uncertainty is smaller than the symbol size. Note that the y axis scale above the sediment-water interface is different from the scale below the interface. The right panel shows bulk sediment composition for the same core and sediment intervals as pore water data ($CaCO_3$ – grey, lithogenic material – brown, organic matter – green; see supplemental section 3.3 and Table S7). The x axis scale has a break between 0% and 70%.

been observed in recent seawater culture experiments (Miletto et al., 2021); however, our data do not unequivocally indicate MnOx-driven cycling, and other potential oxidants may be involved (e.g. H_2O_2, for which data are not available).

Differences between the three incubations may also be related to metal oxides. Incubations from 150 m had much higher pMn than those from shallower depths (Inc. 1, 100 m & Inc. 2; Table S1), following depth trends in oceanic pMn (Ohnemus et al., 2019), and potentially explaining the lack of Cr release in shallower treatments. Particulate Fe in Inc. 1 was higher than in Inc. 3 (Table S1), indicating more Fe-rich mixed oxides, which may impact Cr oxidation and explain differences between these incubations. If particulate MnOx are important, the enriched particle concentrations in the incubations, possibly in combination with the formation of particle aggregates, would help to increase the probability of oxidative Cr release by MnOx relative to ambient seawater conditions. Consequently, if oxidative particulate Cr release is driven by reduction with MnOx, it may be facilitated by more Mn-rich oceanic particles at greater depth (Ohnemus et al., 2019) and in marine sediments, supporting a deeper regeneration cycle for Cr than organic matter.

The increase in [Cr] was accompanied by a statistically significant decrease in δ^{53}Cr in four of six samples (Fig. 2, Table S2). δ^{53}Cr decreases were not significant for the remaining two samples, consistent with the small increase in [Cr]. Inter-replicate variability is likely controlled by small initial differences in biological communities and particle compositions in each cubitainer, hence real natural variability, rather than analytical uncertainty, given differences in [Cr] between triplicates were well outside of analytical uncertainty (Fig. 2, Table S2). This release of low δ^{53}Cr from particles provides evidence for predictions that Cr adsorbed onto biogenic particles is isotopically light (Scheiderich et al., 2015; Semeniuk et al., 2016; Janssen et al., 2020).

A strong linear relationship is observed between δ^{53}Cr and ln[Cr] in the regeneration incubation samples ($r^2 = 0.89$) with an implied enrichment factor (ε) = −0.66‰, matching that implied by the global δ^{53}Cr–[Cr] array (global $\varepsilon \approx -0.70$‰, Fig. 2). This supports release from biogenic particles as an important process in driving global [Cr] and δ^{53}Cr distributions. While proposed earlier (Scheiderich et al., 2015), previous studies have highlighted that biogenic Cr accumulation was lacking strong support in oceanic depth profiles (Scheiderich et al., 2015; Goring-Harford et al., 2018; Moos and Boyle, 2019; Rickli et al., 2019). This study provides the first direct evidence that Cr release from biogenic particles acts as a control on δ^{53}Cr across intermediate and deep waters, and ultimately also supports the inverse of this process – the adsorption of Cr onto biogenic particles in the surface ocean – as a control of δ^{53}Cr and [Cr] (Scheiderich et al., 2015; Semeniuk et al., 2016; Goring-Harford et al., 2018; Janssen et al., 2020).

4.2. Benthic Cr supply: the flux of Cr to bottom waters from pore waters

Pore waters were sampled from calcareous ooze sediments (~3350 m water depth) collected from a shallower feature punctuating the abyssal plain (~4000-5000 m) in the Tasman Basin (Fig. 1). Regional sedimentation rates are on the order of 1-2 cm kyr^{-1} (Cochran and Osmond, 1976). Organic matter is around 1% at the sediment surface, though upper sediments remain oxic and organic carbon content decreases with depth (Table 1, Table S7). Surface sediment Mn/Al (~0.016) and Fe/Al (~0.53) are higher than upper continental crust values (0.009 and 0.48 respectively, Rudnick and Gao, 2003; Table S7), suggesting slight authigenic oxide enrichment.

Pore water dissolved [Cr] shows a shallow sub-surface maximum (0-1 cm below the sea floor) of 47.4 nmol kg^{-1}, approximately an order of magnitude greater than local bottom waters (4.81 nmol kg^{-1}, Fig. 3), and pore water [Cr] decreases with depth. Pore water [Mn] and [Fe] do not show µM level enrichments, reflecting oxic sediment conditions (Fig. 3). The lowest pore water [Cr] is observed in the deepest samples (6.7 nmol kg^{-1} at 9-10 cm depth), which remain elevated relative to bottom water. This upper pore water [Cr] maximum is consistent with observations by Shaw et al. (1990), though in contrast to our data, Shaw et al. (1990) observed Cr removal in the uppermost oxic sediments, above near-

surface pore water [Cr] maxima. The absence of Cr removal in our uppermost oxic sediments may reflect the strong differences in bulk sediment composition between lithogenic-dominated sites (Shaw et al., 1990) and our carbonate-dominated site.

A near-surface pore water [Cr] maximum suggests pore waters act as a diffusive source of dissolved Cr to the ocean. Bottom waters composed of CDW are enriched in [Cr] and are isotopically distinct ([Cr] = 4.81 nmol kg^{-1}, $\delta^{53}Cr = 0.76 \pm 0.03$‰) from CDW at nearby stations not in contact with sediments ([Cr] = 3.95 nmol kg^{-1}, $\delta^{53}Cr = 0.84 \pm 0.03$‰, 2SD, n = 6 samples ≥3000 m at stations TS8 and PS2, Table S9). Given the gradient of [Cr] from the pore water to the overlying bottom water, the diffusive flux of dissolved Cr can be estimated using Equation (1)

$$Flux_{Cr} = D_s \frac{\Delta C}{\Delta z} \quad (1)$$

where D_s is the Cr diffusion coefficient corrected for temperature and tortuosity (supplemental material, see also Abbott et al., 2015), giving an estimated benthic flux of ~3 nmol Cr cm^{-2} yr^{-1}.

To contextualize this, if global oxic sediments were characterized by a benthic source of this magnitude, the global benthic Cr flux would be comparable to or larger than riverine inputs, currently believed to be the dominant Cr source (Bonnand et al., 2013; supplemental material), consistent with box model estimates (Jeandel and Minster, 1987). While quantitative estimates of global benthic Cr fluxes await greater data availability across diverse sediment types, our data identify that benthic sources are at least locally important and support previous studies that: (1) have argued for benthic Cr fluxes based on globally distributed elevated deep water [Cr] (Cranston, 1983; Murray et al., 1983; Jeandel and Minster, 1987), and (2) have invoked elevated pore water [Cr] to explain Cr enrichments in sedimented planktonic foraminifera compared to water column samples (Remmelzwaal et al., 2019).

We use bulk sediment composition to examine potential sources of Cr to pore waters by applying mass balance calculations based on the average composition of the upper 4 cm, reported Cr concentrations of these phases, and regional sedimentation rates (Table 1). These calculations suggest that neither lithogenic, carbonate-hosted, nor surface phytoplankton Cr can account for the Cr flux out of these carbonate-rich and detrital-poor sediments (Table 1). Therefore, we suggest a combination of mechanisms causing Cr enrichments in particles delivered to sediments can explain the observed pore water data. First, respiration may result in relative Cr enrichments in particles reaching the seafloor because the release of Cr from particles appears decoupled from organic matter respiration (see sections 4.1, 4.3). At the same time, scavenging of particle-reactive Cr(III) may increase the Cr content of biogenic and non-biogenic particles. Regardless of which process(es) are involved, the Cr released from these sediments must largely be derived from the water column based on mass balance and is incorporated into the sediments as particle-adsorbed Cr that has been scavenged onto particle surfaces in the upper ocean (Connelly et al., 2006; Semeniuk et al., 2016; Janssen et al., 2020), and at intermediate depths (see section 4.3), while detrital Cr may be more inert. The similar [Cr] and [Mn] profiles in upper pore waters (Fig. 3) may reflect related geochemical controls (e.g. oxidative release of Cr(III) coupled to Mn reduction).

By mass balance calculations using observed bottom and deep water [Cr] and $\delta^{53}Cr$ (bottom water: [Cr] = 4.81 nmol kg^{-1}, $\delta^{53}Cr = 0.76 \pm 0.03$‰; deep water: ([Cr] = 3.95 nmol kg^{-1}, $\delta^{53}Cr = 0.84 \pm 0.03$‰, 2SD; supplemental material), we estimate pore water $\delta^{53}Cr$ at 0.34 ± 0.25‰ (2 SEM propagated error), which is heavier than silicate earth (-0.124 ± 0.101‰, Schoenberg et al., 2008). While the closeness of these ranges indicates that some lithogenic component may contribute to the pore water flux, these data and the likely refractory nature of lithogenic Cr (e.g. Bauer et al., 2019), argue against significant lithogenic Cr contributions to the pore water flux. In contrast, pore water $\delta^{53}Cr$ is lighter than dissolved $\delta^{53}Cr$ in the upper 1000 m ($\delta^{53}Cr \approx 1.1$-$0.9$‰) by a similar amount as the enrichment factor predicted by the global $\delta^{53}Cr$–[Cr] array ($\varepsilon \approx -0.7$‰). In other words, removal of dissolved Cr to particles in the upper 1000 m with $\Delta^{53}Cr_{particulate\text{-}dissolved}$ following the global array would result in $\delta^{53}Cr_{particulate}$ similar to the calculated $\delta^{53}Cr_{pore\ water}$.

Although the exact origin of pore water Cr is hard to discern, our mass balance calculations highlight the importance of internal processes acting to redistribute Cr within the water column, transferring dissolved Cr from upper waters to deep waters. Therefore, the benthic flux may act more as an attenuation of Cr removal associated with particle export than an entirely new Cr source. Pore water data from diverse sediment types are needed to determine whether a truly new contribution from lithogenic material may be regionally important in more lithogenic-rich sediments.

4.3. Accumulation of Cr in intermediate and deep water masses

To investigate the oceanic implications of the mechanistic insights from our incubation and pore water findings, a compilation of globally-distributed [Cr] data is presented along with macronutrients and apparent oxygen utilization (AOU, a quantification of the O_2 used for organic matter respiration) following the northward advection of Southern Ocean water masses (Fig. 4). Intermediate and deep waters are split into three water mass ranges based on hydrographic properties: AAIW, UCDW/PDW and LCDW (Figure S3, Tables S9-S10).

Deeper waters (UCDW and LCDW) show relatively uniform [Cr], AOU and macronutrients at their southern origin, and concentrations increase with northward transport (Fig. 4). However, key differences emerge between tracers primarily reflecting organic matter respiration (AOU, PO_4), phytoplankton frustule-associated $Si(OH)_4$, and [Cr]. AOU and PO_4 consistently show latitudinal maxima in the upper deep water mass (UCDP/PDW) relative to LCDW (Fig. 4). However, $Si(OH)_4$ shows maxima in LCDW, and [Cr] in LCDW is comparable to or higher than in UCDW. These deeper maxima, illustrating an apparent deeper regeneration cycle, may reflect globally important benthic sources as shown for Si (Tréguer and de la Rocha, 2013), consistent with our calculated pore water fluxes and earlier global Cr models (Jeandel and Minster, 1987). Chromium–$Si(OH)_4$ distributions show a stronger correlation (r^2 = 0.58, n = 65) than Cr–AOU (r^2 = 0.44, n = 71) and Cr–PO_4 (r^2 = 0.52, n = 67) (Fig. 5), supporting Cr release from biogenic material as being mechanistically independent from organic matter respiration.

The highest deep water [Cr] to date is found below the ETSP OMZ, where accumulated Cr represents up to ~45% of total deep water [Cr] based on Southern Ocean end members. While suboxic sediments are a net sink term (Moos et al., 2020; Nasemann et al., 2020), these deep water [Cr] enrichments may reflect proximity to a benthic source from deeper oxic sediments (section 4.2, Fig. 1). Deep ETNP samples are also enriched relative to the subtropical South Pacific and subarctic North Pacific (Fig. 4), suggesting a connection to the intense OMZs overlying these deep [Cr] enrichments (Murray et al., 1983; Rue et al., 1997; Moos et al., 2020). Mechanistically, enhanced water column [Cr] removal and export of particulate Cr to depth combined with elevated pMn present below these OMZs (e.g. Murray et al., 1983) would facilitate the oxidative release of Cr from particles in the water column or oxic sediments. This Cr-specific enrichment process would cause deep waters below intense OMZs to deviate from Cr–macronutrient correlations, which is confirmed by the resulting strengthening of the Cr correlation with Si (r^2 = 0.73) when removing samples below the ETSP

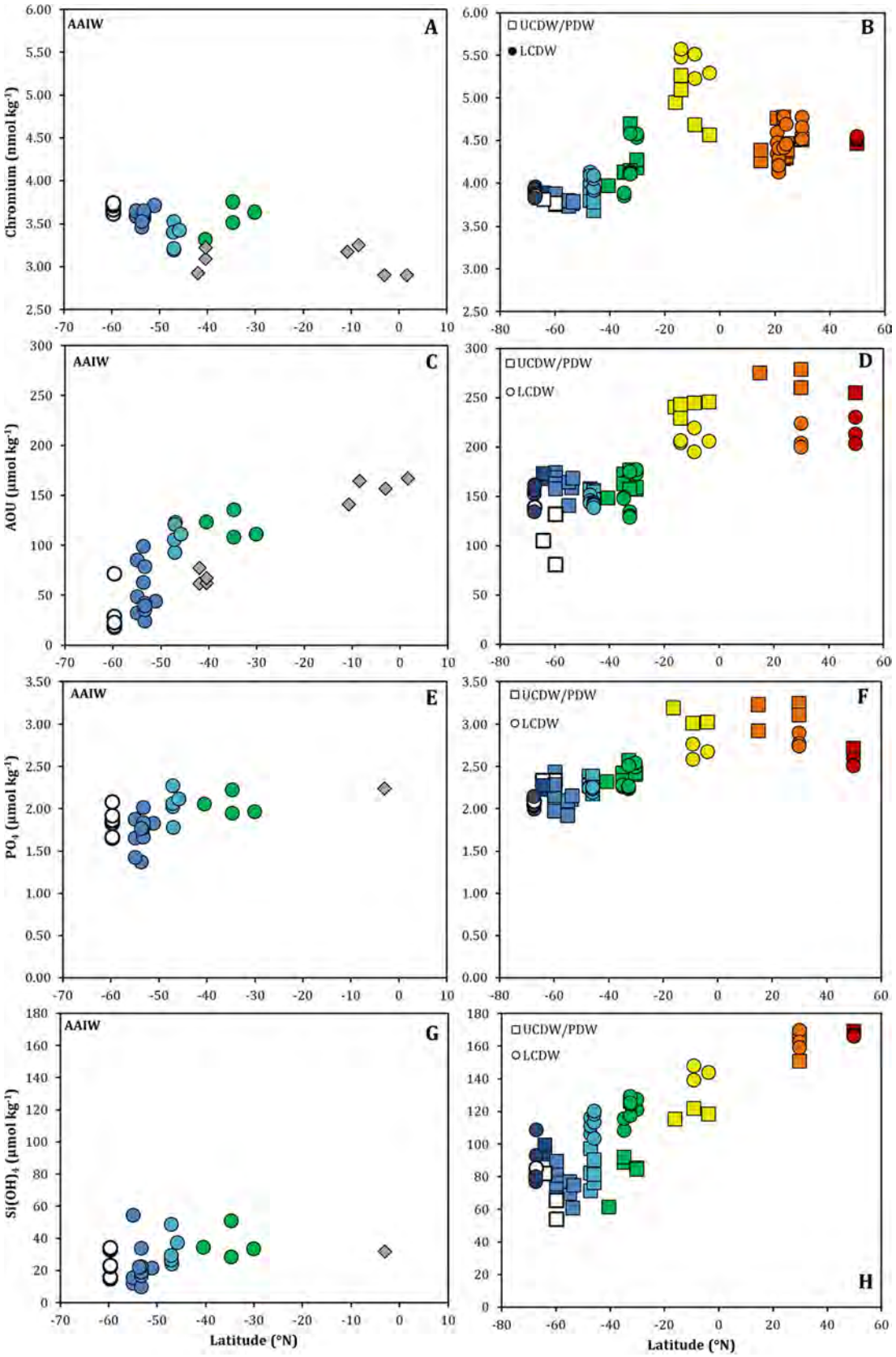

Fig. 4. Chromium and macronutrient concentrations and AOU along intermediate and deep water circulation. Modification of deep water [Cr] is shown, along with parameters associated with the regeneration of organic material ($[PO_4]$, AOU) and dissolution of plankton skeletal/frustule phases ($[Si(OH)_4]$). Panels on the left show AAIW (circles – Southern and Pacific Ocean data, diamonds – Atlantic Ocean data) while panels on the right show Southern and Pacific Ocean UCDW, PDW and LCDW, with UCDW and PDW in circles and LCDW in squares. Open circles denote samples with Antarctic Surface Water or Winter Water contributions. Colors match sampling locations shown in Figs. 1 and S3, and full data and sources are shown in Tables S8-S10. Direct comparisons between [Cr] and AOU, PO_4 and $Si(OH)_4$ are shown in Fig. 5. Note the different x axis ranges for left and right panels.

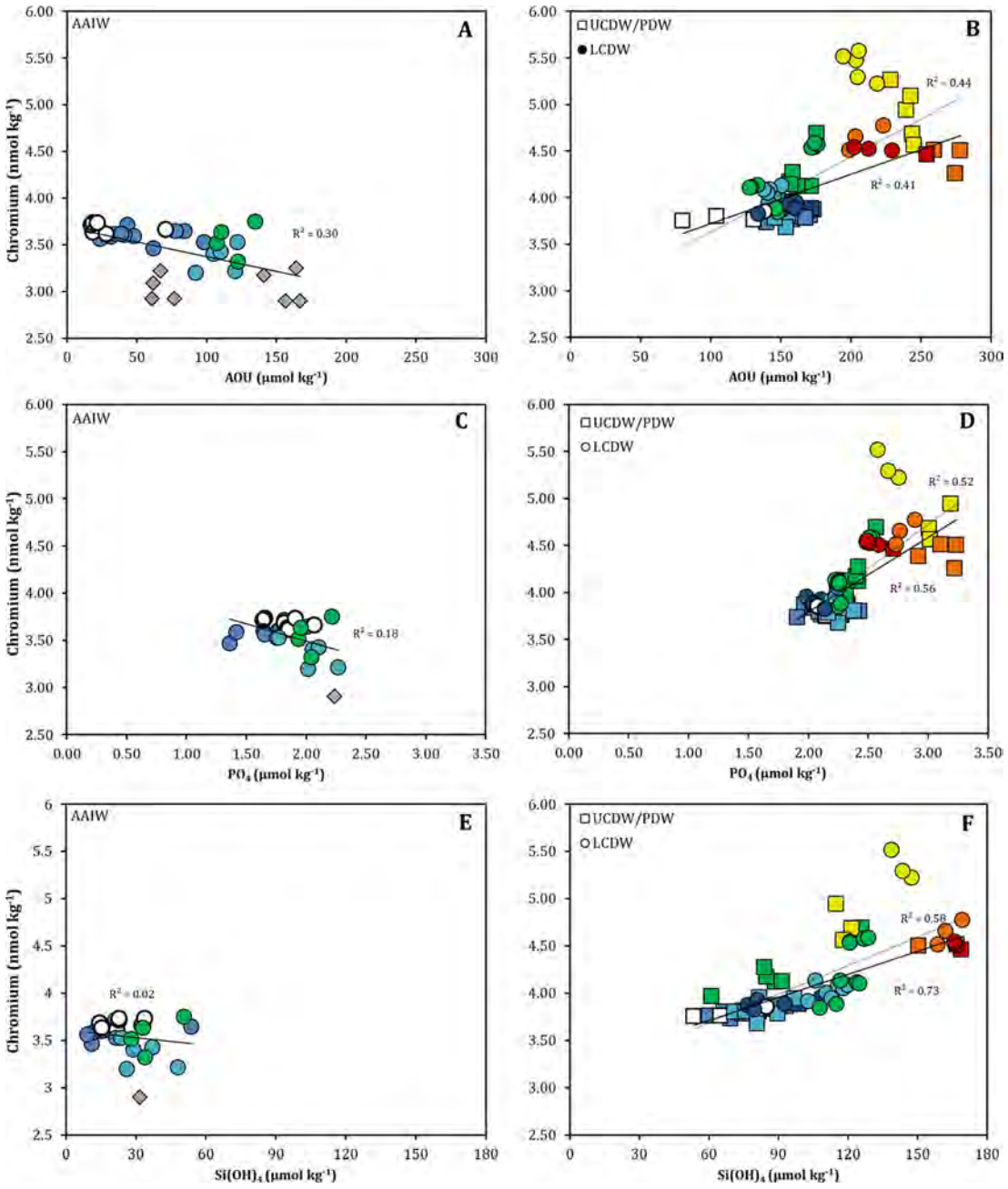

Fig. 5. Chromium–nutrient and Cr–AOU cross plots. Dissolved Cr is shown compared to AOU (A, B), PO_4 (C, D) and $Si(OH)_4$ (E, F) for the intermediate (A, C, E) and deepwater (B, D, F) dataset to highlight decoupling of Cr from tracers of organic matter respiration and regeneration of organic-associated macronutrients (AOU, PO_4). Symbols follow those used in Fig. 4. Dashed lines in panels B, D and E indicate correlations across all data, while solid lines indicate correlations without ETSP data.

OMZ (correlations with PO_4 ($r^2 = 0.56$) and AOU ($r^2 = 0.41$) remain similar; Fig. 5).

Intermediate waters are associated with high carbon respiration with northward advection (Fig. 4). Southern waters with properties similar to newly-formed AAIW show the highest [Cr], and concentrations are generally stable or decrease with northward transport, indicating [Cr] is decoupled from organic matter respiration. A general northward decrease in [Cr] is found for Atlantic AAIW, accompanied by increasing salinity ($r^2 = 0.54$). This trend likely reflects mixing of AAIW with Cr-poor but more saline thermocline waters and NADW (Fig. 6, Rickli et al., 2019). However, the weakness of the correlation likely suggests more complicated mixing of multiple water masses, variable Cr scavenging in intermediate waters, or both.

4.3.1. Implications of water mass [Cr] accumulation trends on Cr–macronutrient coupling in the global ocean

Widely observed Cr–macronutrient correlations suggest shared biogeochemical controls (e.g. Campbell and Yeats, 1981; Cranston, 1983; Jeandel and Minster, 1987; Rickli et al., 2019; Nasemann et al., 2020). Recent studies of other metal–macronutrient associations have highlighted the importance of three dimensional processes, rather than vertical-controlled simplifications, with preformed relationships, scavenging, and variable metal:macronutrient uptake ratios across taxa and nutrient regimes (e.g. Quay et al., 2015; Vance et al., 2017; Ohnemus et al., 2019) driving globally-correlated distributions.

While correlations between [Cr] and PO_4 exist on different spatial scales (e.g. Cranston, 1983; Rickli et al., 2019), biogenic

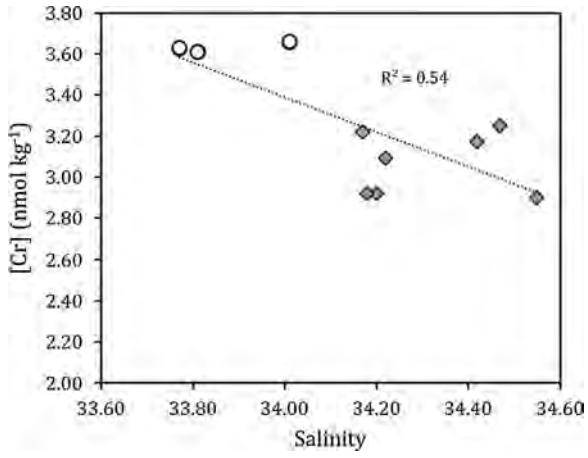

Fig. 6. The impact of mixing on [Cr] in AAIW. Chromium concentrations are shown with salinity for AAIW samples in the Drake Passage (open circles) and the Atlantic Ocean (grey diamonds).

Cr fluxes are low relative to other nutrient-type metals and macronutrients as apparent in smaller surface [Cr] depletions, lower surface-to-deep [Cr] gradients, reduced [Cr] accumulation in global deep water, and [Cr] accumulation in subsurface waters that is independent from organic matter respiration (sections 4.1–4.3, Fig. 5). Therefore observed associations between [Cr] and PO_4 probably reflect mixing between distinct oceanic end-members (see Rickli et al., 2019) rather than coupled vertically-driven processes (e.g. particle sinking and regeneration). Consequently, end-member pre-formed Cr:macronutrient ratios and global circulation would largely shape Cr–macronutrient relationships in the ocean interior and their variability, with end-members impacted by biological uptake at their formation sites.

A prominent benthic source of dissolved Cr provides a mechanistic explanation for [Cr] and $Si(OH)_4$ coupling by vertical processes in addition to water mass mixing. However, deep water data demonstrate that [Cr] and $Si(OH)_4$ can decouple (Figs. 4–5), and local differences in Cr–$Si(OH)_4$ slopes (Jeandel and Minster, 1987) suggest the relationship between Cr and $Si(OH)_4$ may reflect a combination of advection and mixing of waters with different pre-formed Cr:$Si(OH)_4$ ratios, Cr and $Si(OH)_4$ drawdown by phytoplankton in surface waters, and the impact of sediment type and location on benthic dissolved Cr and $Si(OH)_4$ fluxes (e.g. elevated [Cr] below OMZs, Figs. 4–5). Based on these variable controls, and recognizing that circulation likely plays a central role, interpretations of Cr–macronutrient trends within depth profiles should be made with caution.

5. An updated global ocean Cr biogeochemical cycle

The foundations for understanding oceanic δ^{53}Cr distributions were first presented by Scheiderich et al. (2015), who demonstrated a tight coupling between [Cr] and δ^{53}Cr. Building on the [Cr] literature, Scheiderich et al. (2015) hypothesized that δ^{53}Cr distributions reflected the known controls on [Cr]: reduction and removal in OMZs and Cr export with biogenic particle fluxes along with regeneration from biogenic material. Subsequent δ^{53}Cr research has attempted to assess these mechanisms and their associated fractionations to clarify their roles in the global Cr and δ^{53}Cr cycle. We combine these initial hypotheses and recent advancements with our new data to improve our mechanistic understanding of Cr cycling in the global ocean and highlight remaining uncertainties. This set of mechanistic controls defines how internal oceanic processes regulate δ^{53}Cr, forming the global relationship (Fig. 7 panel A), and will help to guide paleoceanographic applications of marine δ^{53}Cr.

Here, we have demonstrated that Cr release from biogenic particles, either in the water column oxic sediments, can explain the [Cr]-rich side of the array (Fig. 7 panels B and C) consistent with previous work on biological uptake shaping the [Cr]-depleted side of the δ^{53}Cr–[Cr] array (Fig. 7 Panel B; Goring-Harford et al., 2018; Janssen et al., 2020). In OMZs, dissolved Cr can be scavenged in the water column (Moos et al., 2020) and at the sediment surface (Moos et al., 2020; Nasemann et al., 2020), a process that largely follows the global array (Fig. 7 Panel D). Mixing will generally act to homogenize process- and source-induced variability, with the specific effect depending on the signatures of mixing water masses (Fig. 7 panel E, see also section S.4, Figure S4 and Rickli et al., 2019). Hydrothermal circulation may also impact [Cr] and δ^{53}Cr in the modern ocean and paleoceanographic interpretations (Holmden et al., 2016), but remains largely unconstrained at present (Fig. 7 panel F).

Coastal environments are more likely to deviate from the global δ^{53}Cr–[Cr] array due to localized influences, including shelf sources (Goring-Harford et al., 2018) (Fig. 7 Panel C), more quantitative removal in shelf OMZs (Nasemann et al., 2020, Fig. 7 Panel D); dilution from meltwater (Scheiderich et al., 2015, Fig. 7 Panel E), and local riverine inputs (Fig. 7 Panel F). Consequently, reconstructions of seawater δ^{53}Cr from coastally-sourced marine sediment records, including continental margins, should be approached with caution as these records may not reflect global ocean conditions for δ^{53}Cr and/or [Cr].

Taken together, the available body of oceanic data indicates that Cr and δ^{53}Cr distributions are controlled by biological adsorption and scavenging onto sinking particles acting across broad spatial scales, with local enhancement in OMZs, and regeneration from particles in the water column and/or oxic sediments. These signals are then transported and mixed through ocean circulation. Consequently, δ^{53}Cr records in marine-origin sediments should reflect the combination of these processes, with both export productivity and OMZ reduction contributing to Cr accumulation in sediments and with temporal δ^{53}Cr records reflecting modification of these processes over time and with changes in global climate, rather than exclusively reflecting changes in O_2 availability. Additional research is needed to understand early sediment diagenesis, as indicated by elevated pore water [Cr], and how this may alter sediment Cr and δ^{53}Cr signals.

6. Conclusions

Our incubation data provide the first direct evidence of Cr release from biogenic particles and demonstrate that this release, which may be driven by Cr oxidation, is mechanistically independent from the regeneration of major elements in organic matter (e.g. C, N, P). Based on Cr geochemistry and our data, a likely Cr oxidant is MnOx, though we cannot conclusively exclude other potential oxidants. Our pore water data indicate large benthic Cr fluxes can be locally important, and are possibly a globally-important component of the ocean's Cr budget. This benthic flux likely reflects the release of Cr scavenged onto particles in the water column, rather than 'new Cr' from the dissolution of lithogenic material. δ^{53}Cr data from both bottom waters and incubations identify that release from biogenic particles follows the global δ^{53}Cr–[Cr] array, demonstrating that Cr release, either in deep waters or surface sediments, can explain the high [Cr] end-member of the global δ^{53}Cr–[Cr] array. Furthermore, the data confirm that biogenic export from the surface ocean and release at depth is important in shaping distributions of both [Cr] and δ^{53}Cr throughout the global ocean. A global compilation provides clear evidence of [Cr] accumulation in deep waters, supporting a deep regeneration cycle for Cr that is decoupled from organic matter respiration, includes a potential benthic source, and is enhanced below tropical

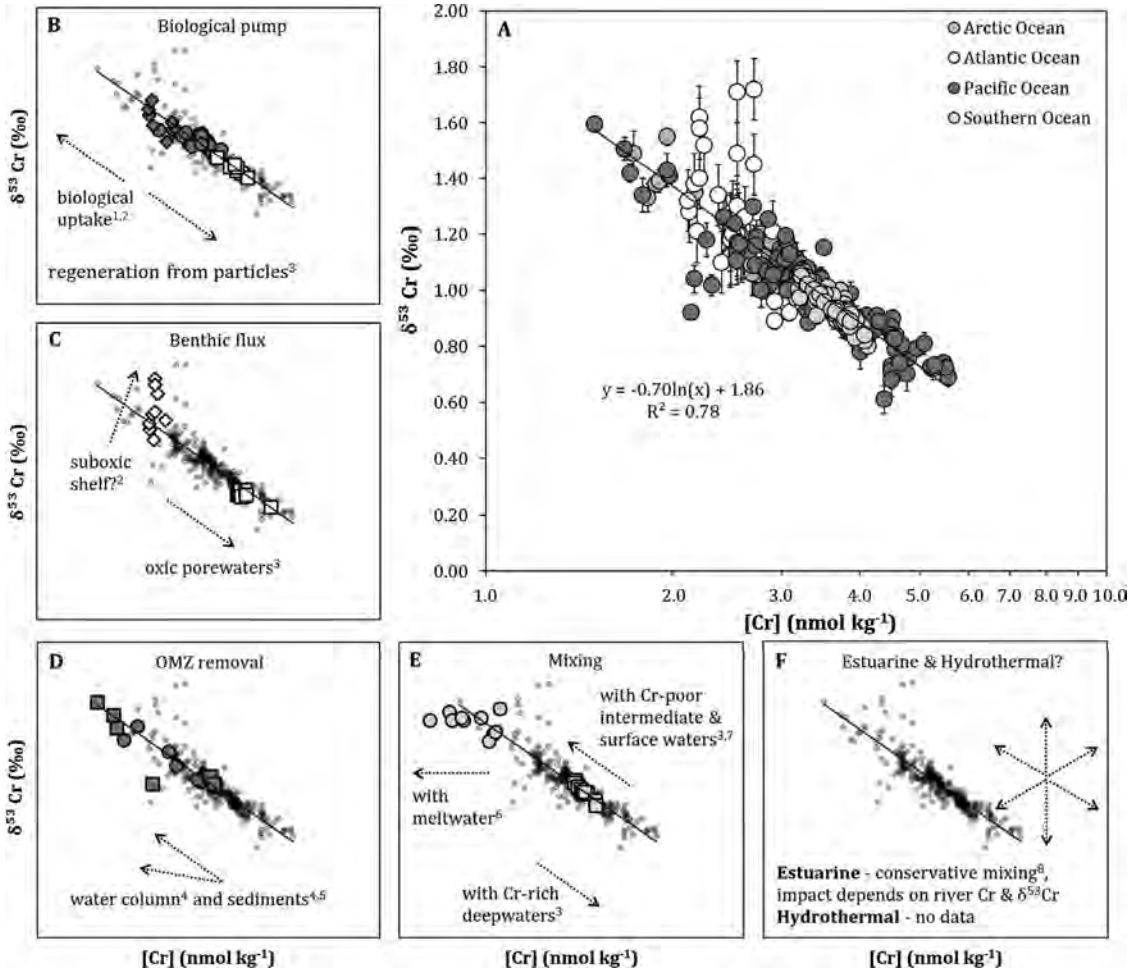

Fig. 7. Toward a mechanistic understanding of the global ocean Cr cycle. The global array of open ocean [Cr] and δ^{53}Cr data is shown (panel A) along with specific subsets of data highlighted to demonstrate how different processes drive the global distribution. References for these subsets are shown by superscripts. Processes which act to increase [Cr] are shown in white and processes which act to decrease [Cr] are shown in dark grey. Mixing, which may increase or decrease [Cr] depending on the point of reference, is shown in light grey. Panel B shows processes within the biological pump (surface uptake, export of biogenic particles, and regeneration at depth). Panel C shows benthic Cr fluxes. Panel D shows Cr removal in OMZs, which may follow the global trend or deviate slightly. Panel E shows mixing processes. Panel F shows processes which are unconstrained at present (hydrothermal fluxes) or which may have variable impact depending on local characteristics (riverine [Cr] and δ^{53}Cr, estuarine mixing). The axes and ranges of all panels are identical. Data from Moos and Boyle (2019) as well as the following studies were used: [1]Janssen et al., 2020 (dark grey circles, panel B); [2]Goring-Harford et al., 2018 (dark grey diamonds, panel B; white diamonds, panel C); [3]This study (white squares, panels B & C), [4]Moos et al., 2020 (dark grey circles, panel D); [5]Nasemann et al., 2020 (dark grey squares, panel D); [6]Scheiderich et al., 2015 (light grey circles, panel E), [7]Rickli et al., 2019 (light grey squares, panel E), [8]Goring-Harford et al., 2018.

Pacific OMZs due to release of OMZ-scavenged Cr in underlying oxic waters and sediments. Intermediate waters show stable or decreasing [Cr] with northward advection, reflecting minimal release from particles and a potential net water column Cr sink via scavenging. Because both [Cr] and δ^{53}Cr are impacted by biological and physical processes, and pore water data indicate active cycling in near-surface sediments, the role of these processes with respect to Cr paleoredox proxy viability should be incorporated into future δ^{53}Cr O_2-reconstruction applications.

CRediT authorship contribution statement

DJJ led the design of the study along with SLJ, with assistance from MJE, who organized trace metal sampling operations for ACE Leg 1 & IN2018V_02 and all operations for IN2018V_04, BST & DCO, who designed and conducted the shipboard incubations, and ANA, who planned coring operations and conducted sediment and pore water sampling for cruise IN2018V_04. DJJ conducted seawater sampling, processed, and analyzed samples from ACE Leg 1, IN2018V_02, IN2018V_04, and Line P cruise 2012-13. SLJ conducted sampling for ACE Leg 2. DJJ processed and analyzed samples from DY110 and ACE Leg 2. MJE assisted in seawater sampling for ACE Leg 1, IN2018V_02 and IN2018V_04. BT and DO analyzed particulate samples from IN2018V_04 regeneration experiments. PN processed and analyzed samples from M77/4. DJJ and DG processed and analyzed samples from GP13. MJE analyzed POC and pore water [Fe] and [Mn] samples. DJJ led interpretations and writing, and all authors contributed to the manuscript.

Declaration of competing interest

The authors declare that they have no known competing financial interests or personal relationships that could have appeared to influence the work reported in this paper.

Data availability

Full cruise CTD and macronutrient data for cruises IN2018V_02 and IN2018V_04 are available from CSIRO (https://www.cmar.csiro.au/data/trawler/). Full macronutrient and CTD data from the ACE transect are available from the ACE collection on Zenodo (https://zenodo.org/communities/spi-ace). Full macronutrient and CTD data

from the M77/4 cruise are available from the Pangaea repository (https://www.pangaea.de/). Full Line P macronutrient and CTD data are available from the Line P website (http://www.waterproperties.ca/linep/data.php). Shipboard incubation data are available in Tables S1-S4. Pore water data are available in Table S5 and sediment data are available in Table S7. New and literature data used for the isopycnal compilation are available in the supplemental material (Tables S9 and S10). All new Cr data in this manuscript are also available in an open access dataset in the Zenodo repository (https://doi.org/10.5281/zenodo.5408613).

Acknowledgements

We thank the captains, crews, and scientific members of the RV *Investigator* cruises IN2018_V02 and IN2018_V04 as well as the trace metal sampling teams, especially Robin Grun, Pamela Barrett, and Kiefer Forsch, the sediment coring team of Kelly-Anne Lawler, Hannah Kumar, Annabel Payne, and Hannah Wilson, and Phil Boyd for coordinating and planning trace metal operations on cruise IN2018_V02. The authors wish to thank the CSIRO Marine National Facility (MNF) for its support in the form of sea time on RV Investigator, support personnel, scientific equipment and data management. We thank the captains, crew, and scientific personnel of the additional cruises from which we present new data (ACE Leg 1, GP13, M77/4, Line P 2012-13, DY110) as well as Christel Hassler and Andy Bowie for samples from cruise GP13, Nina Schuback for sampling on cruise DY110, and Martin Frank and Patricia Grasse for samples from cruise M77/4. We thank Julijana Krbanjevic for TC/TIC analysis. We acknowledge Zanna Chase, Barbara Grose, and Pete Strutton for logistical support, Zanna Chase for the use of her centrifuge on voyage IN2018V_04, and Martin Wille for sharing analytical expertise, Neptune support, and for helpful discussions. We thank Tim Conway for providing CTD data for the SAFe station. This manuscript was improved by constructive comments from the editor Lou Derry and three anonymous reviewers. This work was supported by the Swiss National Science Foundation (SNSF grant PP00P2_172915) and by a European Research Council (ERC) Consolidator Grant (SCrIPT grant agreement 819139) to SLJ. Chromium data were obtained on a Neptune MC-ICP-MS acquired with funds from the NCCR PlanetS supported by SNSF grant 51NF40-141881. Maps and some figures were made using Ocean Data View (available at http://odv.awi.de).

Appendix A. Supplementary material

Supplementary material related to this article can be found online at https://doi.org/10.1016/j.epsl.2021.117163.

References

Abbott, A.N., Haley, B.A., McManus, J., Reimers, C.E., 2015. The sedimentary flux of dissolved rare earth elements to the ocean. Geochim. Cosmochim. Acta 154, 186–200. https://doi.org/10.1016/j.gca.2015.01.010.

Achterberg, E.P., van den Berg, C.M.G., 1997. Chemical speciation of chromium and nickel in the western Mediterranean. Deep-Sea Res., Part 2, Top. Stud. Oceanogr. 44, 693–720. https://doi.org/10.1016/S0967-0645(96)00086-0.

Bauer, K., Cole, D.B., Asael, D., Francois, R., Calvert, S.E., Poulton, S.W., Planavsky, N.J., Crowe, S.A., 2019. Chromium isotopes in marine hydrothermal sediments. Chem. Geol. 529, 119286. https://doi.org/10.1016/j.chemgeo.2019.119286.

Berger, C.J.M., Lippiatt, S.M., Lawrence, M.G., Bruland, K.W., 2008. Application of a chemical leach technique for estimating labile particulate aluminum, iron, and manganese in the Columbia River plume and coastal waters off Oregon and Washington. J. Geophys. Res., Oceans 113, C00B01. https://doi.org/10.1029/2007JC004703.

Bonnand, P., James, R.H., Parkinson, I.J., Connelly, D.P., Fairchild, I.J., 2013. The chromium isotopic composition of seawater and marine sediments. Earth Planet. Sci. Lett. 382, 10–20. https://doi.org/10.1016/j.epsl.2013.09.001.

Bostock, H.C., Sutton, P.J., Williams, M.J.M., Opdyke, B.N., 2013. Reviewing the circulation and mixing of Antarctic Intermediate Water in the South Pacific using evidence from geochemical tracers and Argo float trajectories. Deep-Sea Res., Part 1 73, 84–98. https://doi.org/10.1016/j.dsr.2012.11.007.

Campbell, J.A., Yeats, P.A., 1981. Dissolved chromium in the northwest Atlantic Ocean. Earth Planet. Sci. Lett. 53, 427–433. https://doi.org/10.1016/0012-821X(81)90047-9.

Cochran, J.K., Osmond, J.K., 1976. Sedimentation patterns and accumulation rates in the Tasman Basin. Deep-Sea Res. 23 (3), 193–210. https://doi.org/10.1016/0011-7471(76)91324-3.

Connelly, D.P., Statham, P.J., Knap, A.H., 2006. Seasonal changes in speciation of dissolved chromium in the surface Sargasso Sea. Deep-Sea Res., Part 1 53, 1975–1988. https://doi.org/10.1016/j.dsr.2006.09.005.

Cranston, R.E., 1983. Chromium in Cascadia Basin, northeast Pacific Ocean. Mar. Chem. 13, 109–125. https://doi.org/10.1016/0304-4203(83)90020-8.

Cranston, R.E., Murray, J.W., 1978. Determination of chromium species in natural waters. Anal. Chim. Acta 99, 275–282. https://doi.org/10.1016/S0003-2670(01)83568-6.

Elderfield, H., 1970. Chromium speciation in sea water. Earth Planet. Sci. Lett. 9, 10–16. https://doi.org/10.1016/0012-821X(70)90017-8.

Frei, R., Gaucher, C., Poulton, S.W., Canfield, D.E., 2009. Fluctuations in Precambrian atmospheric oxygenation recorded by chromium isotopes. Nature 461, 250–254. https://doi.org/10.1038/nature08266.

Goring-Harford, H.J., Klar, J.K., Pearce, C.R., Connelly, D.P., Achterberg, E.P., James, R.H., 2018. Behaviour of chromium isotopes in the eastern sub-tropical Atlantic Oxygen Minimum Zone. Geochim. Cosmochim. Acta 236, 41–59. https://doi.org/10.1016/j.gca.2018.03.004.

Holmden, C., Jacobson, A.D., Sageman, B.B., Hurtgen, M.T., 2016. Response of the Cr isotope proxy to Cretaceous Ocean Anoxic Event 2 in a pelagic carbonate succession from the Western Interior Seaway. Geochim. Cosmochim. Acta 186, 277–295. https://doi.org/10.1016/j.gca.2016.04.039.

Huang, T., Moos, S.B., Boyle, E.A., 2021. Trivalent chromium isotopes in the eastern tropical North Pacific oxygen-deficient zone. Proc. Natl. Acad. Sci. USA 118 (8), e1918605118. https://doi.org/10.1073/pnas.1918605118.

Janssen, D.J., Cullen, J.T., 2015. Decoupling of zinc and silicic acid in the subarctic northeast Pacific interior. Mar. Chem. 177, 124–133. https://doi.org/10.1016/j.marchem.2015.03.014.

Janssen, D.J., Rickli, J., Quay, P.D., White, A.E., Nasemann, P., Jaccard, S.L., 2020. Biological control of chromium redox and stable isotope composition in the surface ocean. Glob. Biogeochem. Cycles 34. https://doi.org/10.1029/2019GB006397.

Jeandel, C., Minster, J.F., 1987. Chromium behavior in the ocean: global versus regional processes. Glob. Biogeochem. Cycles 1, 131–154. https://doi.org/10.1029/GB001i002p0013.

Kawabe, M., Fujio, S., 2010. Pacific Ocean circulation based on observation. J. Oceanogr. 66, 389–403. https://doi.org/10.1007/s10872-010-0034-8.

Larqué, L., Maamaatuaiahutapu, K., Garçon, V., 1997. On the intermediate and deep water flows in the South Atlantic Ocean. J. Geophys. Res., Oceans 106 (C6), 12425–12440. https://doi.org/10.1029/97JC00629.

Martin, J.H., Knauer, G.A., 1973. The elemental composition of plankton. Geochim. Cosmochim. Acta 37 (7), 1639–1653. https://doi.org/10.1016/0016-7037(73)90154-3.

Mayer, L.M., Schick, L.L., Chang, C.A., 1984. Incorporation of trivalent chromium into riverine and estuarine colloidal material. Geochim. Cosmochim. Acta 48 (9), 1717–1722. https://doi.org/10.1016/0016-7037(84)90027-9.

Miletto, M., Wang, X., Planavsky, N.J., Luther, G.W., Lyons, T.W., Tebo, B.M., 2021. Marine microbial Mn(II) oxidation mediates Cr(III) oxidation and isotope fractionation. Geochim. Cosmochim. Acta 297, 101–119. https://doi.org/10.1016/j.gca.2021.01.008.

Moos, S.B., Boyle, E.A., 2019. Determination of accurate and precise chromium isotope ratios in seawater samples by MC-ICP-MS illustrated by analysis of SAFe Station in the North Pacific Ocean. Chem. Geol. 511, 481–493. https://doi.org/10.1016/j.chemgeo.2018.07.027.

Moos, S.B., Boyle, E.A., Altabet, M.A., Bourbonnais, A., 2020. Investigating the cycling of chromium in the oxygen deficient waters of the Eastern Tropical North Pacific Ocean and the Santa Barbara Basin using stable isotopes. Mar. Chem. 221, 103756. https://doi.org/10.1016/j.marchem.2020.103756.

Mugo, R.K., Orians, K.J., 1993. Seagoing method for the determination of chromium(III) and total chromium in sea water by electron-capture detection gas chromatography. Anal. Chim. Acta 271 (1), 1–9. https://doi.org/10.1016/0003-2670(93)80545-V.

Murray, J.W., Spell, B., Paul, B., 1983. The contrasting geochemistry of manganese and chromium in the eastern tropical Pacific Ocean. In: Wong, C.S., Boyle, E., Bruland, K.W., Burton, J.D., Goldberg, E.D. (Eds.), Trace Metals in Sea Water. In: NATO Conference Series (IV Marine Sciences), vol. 9. Springer, Boston, MA, pp. 643–669.

Nasemann, P., Janssen, D.J., Rickli, J., Grasse, P., Franck, M., Jaccard, S.L., 2020. Chromium reduction and associated stable isotope fractionation restricted to anoxic shelf waters in the Peruvian Oxygen Minimum Zone. Geochim. Cosmochim. Acta 285, 207–224. https://doi.org/10.1016/j.gca.2020.06.027.

Ohnemus, D.C., Torrie, R., Twining, B.S., 2019. Exposing the distributions and elemental associations of scavenged particulate phases in the ocean using basin-scale multi-element data sets. Glob. Biogeochem. Cycles 33 (6), 725–748. https://doi.org/10.1029/2018GB006145.

Orsi, A.H., Whitworth III, T., Nowlin Jr, W.D., 1995. On the meridional extent and fronts of the Antarctic Circumpolar Current. Deep-Sea Res., Part 1 42, 641–673. https://doi.org/10.1016/0967-0637(95)00021-W.

Oze, C., Bird, D.K., Fendorf, S., 2007. Genesis of hexavalent chromium from natural sources in soil and groundwater. Proc. Natl. Acad. Sci. USA 104 (16), 6544–6549. https://doi.org/10.1073/pnas.0701085104.

Pettine, M., D'Ottone, L., Campanella, L., Millero, F.J., Passino, R., 1998. The reduction of chromium (VI) by iron (II) in aqueous solutions. Geochim. Cosmochim. Acta 62 (9), 1509–1519. https://doi.org/10.1016/S0016-7037(98)00086-6.

Pettine, M., Millero, F.J., La Noce, T., 1991. Chromium (III) interactions in seawater through its oxidation kinetics. Mar. Chem. 34 (1–2), 29–46. https://doi.org/10.1016/0304-4203(91)90012-L.

Quay, P., Cullen, J., Landing, W., Morton, P., 2015. Processes controlling the distributions of Cd and PO_4 in the ocean. Glob. Biogeochem. Cycles 29 (6), 830–841. https://doi.org/10.1002/2014GB004998.

Rauschenberg, S., Twining, B.S., 2015. Evaluation of approaches to estimate biogenic particulate trace metals in the ocean. Mar. Chem. 171, 67–77. https://doi.org/10.1016/j.marchem.2015.01.004.

Remmelzwaal, S.R.C., Sadekov, A.Y., Parkinson, I.J., Schmidt, D.N., Titelboim, D., Abramovich, S., Roepert, A., Kienhuis, M., Polerecky, L., Goring-Harford, H., et al., 2019. Post-depositional overprinting of chromium in foraminifera. Earth Planet. Sci. Lett. 515, 100–111. https://doi.org/10.1016/j.epsl.2019.03.001.

Rickli, J., Janssen, D.J., Hassler, C., Ellwood, M.J., Jaccard, S.L., 2019. Chromium biogeochemistry and stable isotope distribution in the Southern Ocean. Geochim. Cosmochim. Acta 262, 188–206. https://doi.org/10.1016/j.gca.2019.07.033.

Rudnick, R.L., Gao, S., 2003. 3.01 - Composition of the continental crust. In: Holland, H.D., Turekian, K.K. (Eds.), Treatise on Geochemistry. Pergamon, Oxford, pp. 1–64.

Rue, E.L., Smith, G.J., Cutter, G.A., Bruland, K.W., 1997. The response of trace element redox couples to suboxic conditions in the water column. Deep-Sea Res., Part 1 44 (1), 113–134. https://doi.org/10.1016/S0967-0637(96)00088-X.

Scheiderich, K., Amini, M., Holmden, C., Francois, R., 2015. Global variability of chromium isotopes in seawater demonstrated by Pacific, Atlantic, and Arctic Ocean samples. Earth Planet. Sci. Lett. 423, 87–97. https://doi.org/10.1016/j.epsl.2015.04.030.

Schoenberg, R., Zink, S., Staubwasser, M., von Blanckenburg, F., 2008. The stable Cr isotope inventory of solid Earth reservoirs determined by double spike MC-ICP-MS. Chem. Geol. 249, 294–306. https://doi.org/10.1016/j.chemgeo.2008.01.009.

Semeniuk, D.M., Maldonado, M.T., Jaccard, S.L., 2016. Chromium uptake and adsorption in marine phytoplankton - implications for the marine chromium cycle. Geochim. Cosmochim. Acta 184, 41–54. https://doi.org/10.1016/j.gca.2016.04.021.

Shaw, T.J., Gieskes, J.M., Jahnke, R.A., 1990. Early diagenesis in differing depositional environments: the response of transition metals in pore water. Geochim. Cosmochim. Acta 54 (5), 1233–1246. https://doi.org/10.1016/0016-7037(90)90149-F.

Suga, T., Taley, L.D., 1995. Antarctic Intermediate Water circulation in the tropical and subtropical South Atlantic. J. Geophys. Res., Oceans 100 (C7), 13441–13453. https://doi.org/10.1029/95JC00858.

Talley, L.D., Pickard, G.L., Emery, W.J., Swift, J.H., 2011. Chapter 13 - Southern Ocean. In: Talley, L.D., Pickard, G.L., Emery, W.J., Swift, J.H. (Eds.), Descriptive Physical Oceanography, sixth edition. Academic Press, London, pp. 437–471.

Tréguer, P.J., de la Rocha, C.L., 2013. The world ocean silica cycle. Annu. Rev. Mar. Sci. 5, 477–501. https://doi.org/10.1146/annurev-marine-121211-172346.

Trull, T.W., Bray, S.G., Manganini, S.J., Honjo, S., Francois, R., 2001. Moored sediment trap measurements of carbon export in the Subantarctic and Polar Frontal zones of the Southern Ocean, south of Australia. J. Geophys. Res., Oceans 106 (C12), 31489–31509. https://doi.org/10.1029/2000JC000308.

Twining, B.S., Baines, S.B., 2013. The trace metal composition of marine phytoplankton. Annu. Rev. Mar. Sci. 5, 191–215. https://doi.org/10.1146/annurev-marine-121211-172322.

van der Weijden, C.H., Reith, M., 1982. Chromium(III) — chromium(VI) interconversions in seawater. Mar. Chem. 11 (6), 565–572. https://doi.org/10.1016/0304-4203(82)90003-2.

Vance, D., Little, S.H., de Souza, G.F., Khatiwala, S., Lohan, M.C., Middag, R., 2017. Silicon and zinc biogeochemical cycles coupled through the Southern Ocean. Nat. Geosci. 10, 202–206. https://doi.org/10.1038/ngeo2890.

Wanner, C., Sonnenthal, E.L., 2013. Assessing the control on the effective kinetic Cr isotope fractionation factor: a reactive transport modeling approach. Chem. Geol. 337–338, 88–98. https://doi.org/10.1016/j.chemgeo.2012.11.008.

Wilks, J.V., Rigual-Hernández, A.S., Trull, T.W., Bray, S.G., Flores, J.A., Armand, L.K., 2017. Biogeochemical flux and phytoplankton succession: a year-long sediment trap record in the Australian sector of the Subantarctic zone. Deep-Sea Res., Part 1 121, 143–159. https://doi.org/10.1016/j.dsr.2017.01.001.

Wynn-Edwards, C.A., Shadwick, E.H., Davies, D.M., Bray, S.G., Jansen, P., Trinh, R., Trull, T.W., 2020. Particle fluxes at the Australian Southern Ocean time series (SOTS) achieve organic carbon sequestration at rates close to the global median, are dominated by biogenic carbonates, and show no temporal trends over 20-years. Front. Earth Sci. 8 (329). https://doi.org/10.3389/feart.2020.00329.

Zink, S., Schoenberg, R., Staubwasser, M., 2010. Isotopic fractionation and reaction kinetics between Cr(III) and Cr(VI) in aqueous media. Geochim. Cosmochim. Acta 74 (20). https://doi.org/10.1016/j.gca.2010.07.015.